Galactic origin of ultrahigh energy cosmic rays

V. N. Zirakashvili,[1] V. S. Ptuskin,[2] and S. I. Rogovaya[1]

[1]*Pushkov Institute of Terrestrial Magnetism, Ionosphere and Radiowave Propagation, 108840 Troitsk, Moscow, Russia*

[2]*Institute for Physical Science and Technology, University of Maryland, College Park, Maryland 20742, USA*

(Received 11 May 2024; accepted 3 June 2024; published 11 July 2024)

It is shown that the acceleration of particles by a powerful relativistic jet associated with the activity of a supermassive black hole in the Galactic Center several million years ago may explain the observed cosmic ray spectrum at energies higher than 10^{15} eV. The accelerated particles are efficiently confined in the extended magnetized gas halo created by the supernova and central black hole activity just after the formation of the Galaxy. We found that both the heavy and light chemical composition of ultrahigh energy cosmic rays can be consistent with observations.

DOI: 10.1103/PhysRevD.110.023016

I. INTRODUCTION

The prevailing point of view is that the origin of observed ultrahigh energy cosmic rays (UHECRs) is extragalactic. It is primarily due to the observations of astronomical objects with high energetics, which is required for accelerating to ultrahigh energies, in other galaxies. These are jets in active galactic nuclei (AGN), gamma-ray bursts, tidal disruption events, etc. [1–3].

However, such objects are at times present in our Galaxy. In particular *Fermi* and *eROSITA* bubbles [4,5] are probably linked with the past activity of a supermassive black hole (SMBH) in the Galactic Center. Cosmological simulations of the Milky Way and Andromeda-like galaxies [6] demonstrated periodic activity of a SMBH every 10^8 yr with a peak mechanical luminosity of about 10^{44} erg s^{-1}.

If so, some amount of high energy cosmic rays may have been produced during the periods of activity. Models of this kind have already been suggested in the past [7–14]. The possibility to observe these cosmic rays critically depends on the confinement of particles in the Galaxy.

It appears that this confinement has the potential to be better than previously thought. It is known now that the Milky Way and other galaxies are surrounded by huge halos of hot gas [15]. The gas contains both primordial accreting gas and Galactic gas that was ejected from the Galaxy during early epochs of enhanced star formation and SMBH activity. Since the Galactic magnetic fields were also ejected by the outflows we expect rather effective confinement of particles in such extended (several hundred kpc in size) halos.

Our preliminary model of the acceleration and propagation of UHECRs from nearby SMBHs in the Galactic Center and Andromeda galaxy [16] (Paper I) is further elaborated in the present paper. Three components of particles accelerated in the jet were considered in this model. The lowest energy particles are accelerated at the bow shock of the jet by the diffusive shock acceleration (DSA) mechanism [17–20]. The highest energy particles are accelerated in the jet itself via the shear acceleration [21,22] or via DSA at the termination shock of the jet. For spectral continuity, a third *intermediate* component of accelerated particles was introduced. It could be related to the acceleration in the turbulent jet cocoon or the acceleration in the SMBH magnetosphere [23–26].

In the present paper, we concentrate on the propagation of UHECRs from the Galactic Center and check whether it could considerably contribute to the observed spectrum of UHECRs.

The paper is organized as follows: In the next Sec. II, we in brief outline [16]. Section III provides a description of magnetic fields in the Galactic halo. Section IV presents the numerical results for the propagation of particles from the Galactic Center. Sections V and VI contain the discussion of results and conclusions. The Appendix describes the numerical modeling of the extended gaseous Galactic halo.

II. MODEL OF COSMIC RAY ACCELERATION AND PROPAGATION

A detailed description of our model can be found in Paper I. The calculations of cosmic ray propagation include the spatial diffusion, energy losses, and nuclei fragmentation of protons and nuclei traveling from the central instantaneous point source. The source produces three components of accelerated particles. Each component has a spectrum that is described by the equation

TABLE I. Parameters of the source components in the Galactic Center for the model "light."

Component	γ	$\epsilon_{\max}$	$L_{\mathrm{cr}}(E>1\ \mathrm{GeV})$	$E_{\mathrm{cr}}(E>1\ \mathrm{GeV})$	$k(A)/k_{\odot}(A)$
Jet	1.0	4×10^{19} eV	1.3×10^{37} erg s^{-1}	4×10^{52} erg	$4, A=4, 2(A/Z)^2, A>4$
Bow shock	2.2	6×10^{15} eV	6.9×10^{39} erg s^{-1}	2.2×10^{55} erg	$2, A=4, A/4, A>16,\ 2A/Z, 4<A\le16$
Inner jet	2.2	2×10^{18} eV	2.1×10^{39} erg s^{-1}	6.6×10^{54} erg	$0, A>1$

TABLE II. Parameters of the source components in the Galactic Center for the model "heavy."

Component	γ	$\epsilon_{\max}$	$L_{\mathrm{cr}}(E>1\ \mathrm{GeV})$	$E_{\mathrm{cr}}(E>1\ \mathrm{GeV})$	$k(A)/k_{\odot}(A)$
Jet	1.0	5×10^{18} eV	6.2×10^{37} erg s^{-1}	2.0×10^{53} erg	$4, A=4, 80, A>4$
Bow shock	2.0	4×10^{15} eV	1.1×10^{40} erg s^{-1}	3.5×10^{55} erg	$2, A=4, A/4, A>16,\ 2A/Z, 4<A\le16$
Inner jet	2.0	1.3×10^{18} eV	1.9×10^{39} erg s^{-1}	6×10^{54} erg	$0, A>1$

$$q(\epsilon, A) \propto k(A)\epsilon^{-\gamma}\exp\left(-\frac{A\epsilon}{Z\epsilon_{\max}}\right), \qquad (1)$$

where ϵ is the energy per nucleon, A and Z are the atomic mass and charge numbers, respectively, the function $k(A)$ describes the source chemical composition and can be written in terms of the solar composition $k_{\odot}(A)$.

The parameters of the source spectra are given in Tables I and II, as explained below.

Figure 1 shows the schematic view of the jet. The jet drives a bow shock in the interstellar medium. This shock accelerates particles through the DSA mechanism. The chemical composition of accelerated particles depends on the chemical composition of the interstellar medium and the enrichment due to the preferential injection of ions in comparison to protons. It was found in the hybrid modeling of collisionless shocks [27] that this enrichment is proportional to the ratio of the atomic mass to the charge of injected ions. Thus we expect that function $k(A) = 2k_{\odot}(A)$ for fully ionized He ions. When it comes to heavier ions, we take into account an enhanced metallicity 2 of the Galactic bulge [28] and assume that ions are strongly ionized up to the charge number 8 by a powerful x-ray radiation from the accretion disk. This gives $k(A) = Ak_{\odot}(A)/4$ for ions heavier than Oxygen and $k(A) = 4k_{\odot}(A)$ for lighter ions. In other words, the ions of the Carbon, Nitrogen, and Oxigen (CNO) group are fully ionized.

The highest energy particles are accelerated in the jet itself. The most probable mechanism is the shear acceleration that occurs in the vicinity of the boundary between the jet and the surrounding medium [29]. We assume that the injected ions are fully ionized in the jet.

To maintain spectral continuity, a third intermediate component with light composition is necessary. In the present paper, we consider a pure proton third component. The existence of this component is validated by observations. It is known that particles are accelerated in the vicinity of the SMBH and we observe a variable in time radio, x-ray, and gamma emission in jets [30]. Although this emission is probably of leptonic origin, the acceleration of protons and nuclei is also highly probable. The association of observed astrophysical neutrino events with blazars supports this scenario [31]. An important point is that accelerated nuclei are fully photodisintegrated and

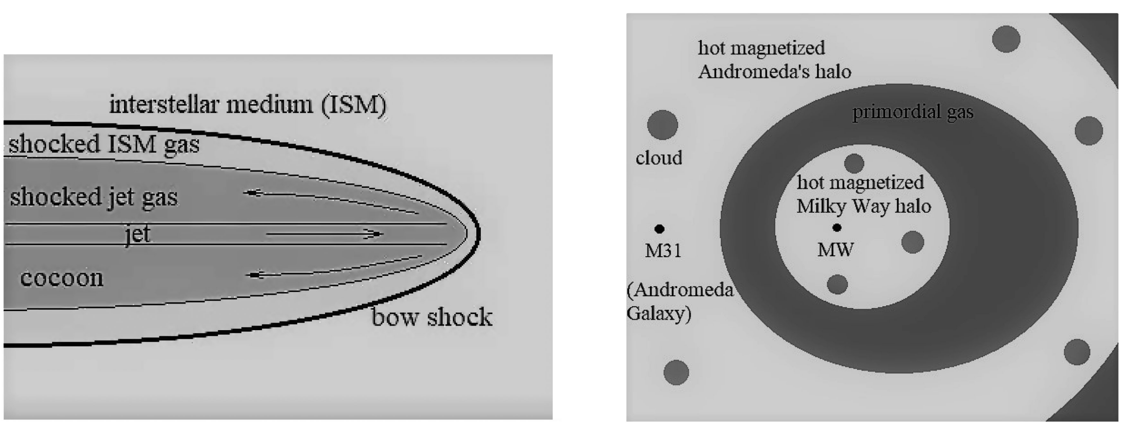

FIG. 1. Schematic view of the jet (left panel) and hot magnetized halos of the Milky Way (MW) and Andromeda galaxy (M31) (right panel).

protons are subject to energy losses in the strong radiation field. They escape the jet via the neutron production mechanism [32]. Because neutrons don't interact with magnetic fields, the spectrum of escaped neutrons is similar to the proton spectrum inside the jet. Later the neutrons decay and turn into protons. As for the acceleration mechanism, it can be either shear acceleration or acceleration during multiple magnetic reconnection events [33]. The latter seems to be possible close to SMBHs where the jet is Pointing dominated.

The shear acceleration can reaccelerate the low energy protons and nuclei of the intermediate component at large distances from the SMBH when the radiation field is not strong. In this regard, there is a correlation between the intermediate and the highest energy components. There is an additional enrichment of nuclei by a factor of $(A/Z)^{\Delta\gamma}$ related to this reacceleration. Here $\Delta\gamma \approx 1$ is the difference of spectral indexes. This gives $k(A) = 4k_{\odot}(A)$ for fully ionized Helium ions and $k(A) = 2(A/Z)^2 k_{\odot}(A)$ for fully ionized heavier ions of the highest energy jet component. The additional factor 2 comes from the higher metallicity of the Galactic bulge.

To describe particle diffusion, we use an analytical approximation of the diffusion coefficient in an isotropic random magnetic field with the Kolmogorov spectrum [34],

$$D = \frac{cl_c}{3}\left(4\frac{E^2}{E_c^2} + 0.9\frac{E}{E_c} + 0.23\frac{E^{1/3}}{E_c^{1/3}}\right),$$
$$E_c = ZeBl_c = 0.9\ \mathrm{EeV} \times ZB_{\mu\mathrm{G}} l_{c,\mathrm{kpc}}, \tag{2}$$

where E is the energy of the particle, B is the magnetic field strength and l_c is the correlation length of the magnetic field. At large energies $E \gg E_c$ the scattering of particles occurs on the magnetic inhomogeneities with scales smaller than the particle gyroradius and the diffusion coefficient is proportional to E^2. At lower energies $E \ll E_c$ the resonant scattering results in the energy dependence of diffusion $\sim E^{1/3}$.

III. HOT MAGNETIZED GALACTIC HALOS

Rapid energy release and the creation of strong outflows (galactic winds) are the results of an enhanced star formation and accretion onto the central supermassive black hole shortly after a galaxy formation. A developing cavity was created in the circumgalactic medium by a hot gas that was ejected and heated by a wind termination shock. In cosmological models, galaxies with strong AGN feedback are shown to have extended "bubbles" of multi-Mpc size, whereas galaxies with a weaker supernova feedback have smaller bubbles of sub-Mpc size [35]. Figure 1 depicts a schematic view of the halos that are thought to have evolved around the Milky Way and Andromeda galaxy.

Galactic magnetic fields are also ejected by the outflows [36]. It is expected that they are amplified by a so-called Cranfill effect [37,38] downstream of the termination shock. Although the gas energy density is higher than the magnetic energy density just downstream of the termination shock, the radial contraction in the incompressible expansion flow results in the amplification of the nonradial components of the magnetic field. The magnetic field strength increases proportional to the distance. As a result, the thermal and magnetic energies are comparable at large distances, see the Appendix. We expect isotropy of the random fields because of the turbulent gas motions generated by clouds of accreting colder and denser circum-Galactic gas inside the bubble of the shocked Galactic gas.

We can obtain a rough estimate of the magnetic field strength in the Milky Way extended halo. It is assumed that 1% of the Galactic 10^{11} stars ended their lives as supernovae. For the standard supernova energy 10^{51} erg, we obtain the total energy of 10^{60} erg. In addition, our SMBH in the Galactic Center has the mass $4 \times 10^6 M_{\odot}$ and the corresponding rest mass energy 7×10^{60} erg. Assuming that 10% of this energy goes into the outflows during SMBH growth and taking into account 30% of the supernova energy we obtain a total of 10^{60} erg. Then the total energy density of the gas and magnetic field is equal to $1.3 \times 10^{-13}\ \mathrm{erg\,cm^{-3}}$ for the bubble radius $R = 400$ kpc. The corresponding equipartition magnetic field strength is 1.3 μG.

Note that the mean magnetic field strength of 0.5 μG along the line of sight at 100 kpc galactocentric distances was estimated from the recent measurements of the Faraday rotation performed for different samples of galaxies [39,40]. The actual value can be higher because of the field reversals and a lower gas number density than assumed $n = 10^{-4}\ \mathrm{cm^{-3}}$. Hence our rough estimate is in accordance with observations.

IV. NUMERICAL RESULTS

We model the propagation of particles in the spherical simulation domain with radius $R = 400$ kpc where an absorbing boundary condition is set. It is assumed that the Galactic Center source is in active phase every 100 million years. The age T of the *Fermi* and *eROSITA* bubbles considered as a result of the last active phase is not exactly known. We analyze two models of bubble formation at $T = 3$ ("light") and $T = 15$ ("heavy") million years ago. The parameters of the source spectrum are adjusted to reproduce observations and are given in Tables I and II. They contain the cosmic ray energy of every energetic component E_{cr} per one activity event and the mean cosmic ray luminosity L_{cr} averaged over 100 million years. The contribution of the Galactic Center in observed UHECRs is dominated by the last active event while more ancient events are important for extragalactic contribution, see below.

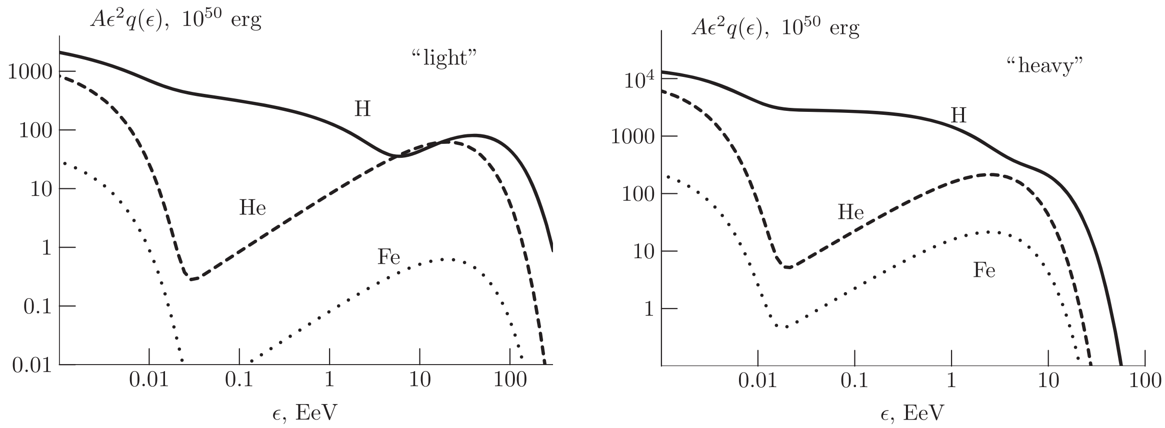

FIG. 2. Source spectra of protons (solid line), He nuclei (dashed line), and Iron (dotted line) produced in the Galactic Center in models "light" (left panel) and "heavy" (right panel).

The source spectra of protons and nuclei are shown in Fig. 2.

For the model "light" the enrichment of the highest energy jet component by heavy nuclei is not needed because Helium nuclei have no time for the photodisintegration. The random magnetic field strength $B = 1$ μG and the correlation length $l_c = 80$ kpc are accepted. For the model "heavy" we use lower values of the magnetic field strength $B = 0.5$ μG and the correlation length $l_c = 40$ kpc. The heavy nuclei in the model "heavy" are 10 times more abundant in comparison to the model "light." This is because these nuclei contain only 1% of mass in the interstellar medium and this is not enough to explain the chemical composition of observed UHECRs.

For such magnetic field and correlation length the scattering free path of particles λ is small enough to justify the use of the diffusion approximation. For example, it is close to $\lambda = 130$ kpc for highest energy Helium nuclei with energy $E = 7 \times 10^{19}$ eV in the model "light."

We also calculate a possible extragalactic contribution for both models. We use in this case the simulation domain with a radius $R = 2.4$ Mpc and a reflecting boundary condition that is a zero gradient of cosmic ray distribution at the boundary. This implies the mean distance 4.8 Mpc between extragalactic sources and corresponds to the source number density of 0.01 Mpc^{-3}. All sources have identical spectra shown in Fig. 2. The particles are released every 100 Myrs. The magnetic field strength $B = 10^{-10}$ G was assumed in this case.

The calculation is performed up to the maximum redshift $z = 1$ in a flat universe with the matter density $\Omega_m = 0.3$, the dark energy density $\Omega_\Lambda = 0.7$, and the Hubble parameter $H = 70\,\mathrm{km\,s^{-1}\,Mpc^{-1}}$ at the current epoch. The strong evolution of sources with a factor $(1 + z)^4$ is taken into account.

For calculations of distribution for atmospheric depth of shower maximum $X_{\max}$ we use the analytical parametrization from [41,42].

The results are shown in Figs. 3–7.

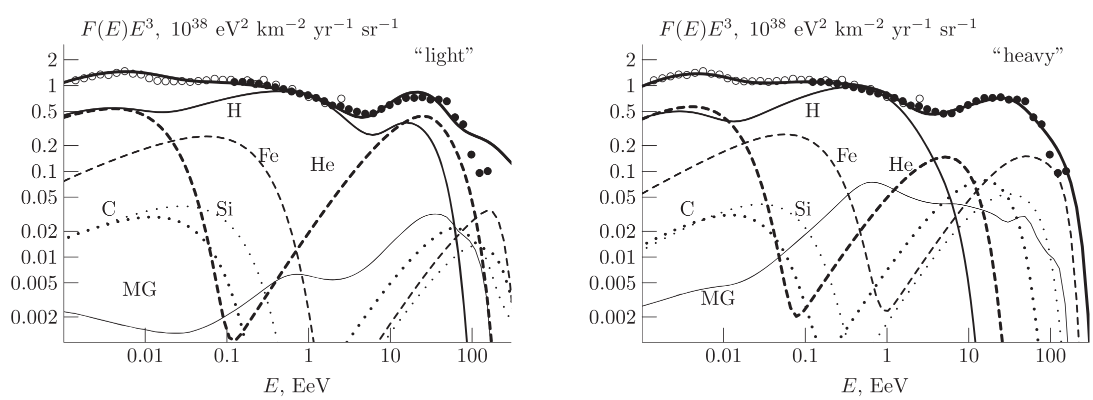

FIG. 3. Spectra of different elements and all-particle spectrum (thick solid line) produced in the Galactic Center and observed at the Earth position in models "light" (left panel) and "heavy" (right panel). A possible metagalactic contribution in the all-particle spectrum (MG) is shown by the thin solid line. Spectra of Tunka-25, Tunka-133 array ([43], open circles), and PAO ([44], energy shift +10%, black circles) are also shown.

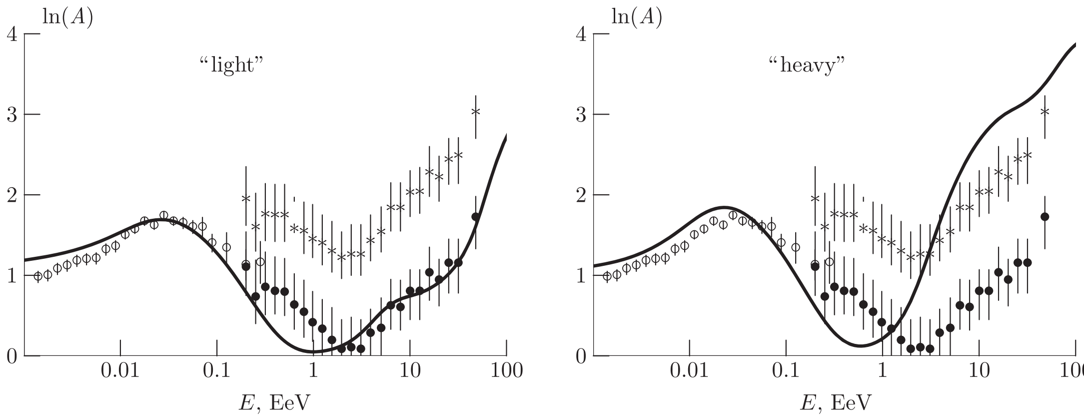

FIG. 4. Calculated mean logarithm of atomic number A (solid line) for the model "light" (left panel) and model "heavy" (right panel). The measurements of Tunka-133, TAIGA-HiSCORE array ([45] open circles), and PAO [hadronic interaction model QGSJetII-04 (black circles) and SIBYLL2.3 (asterisks), energy shift +10% [46]] are also shown.

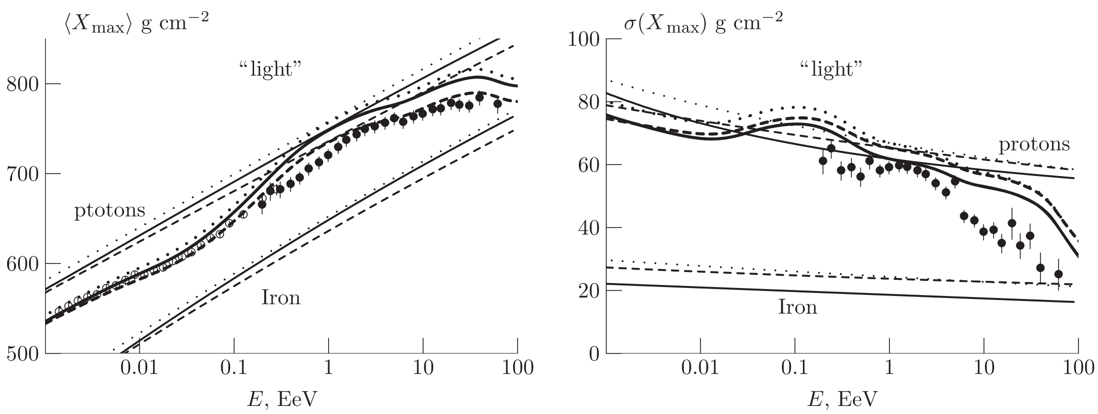

FIG. 5. Calculated mean atmospheric depth of shower maximum $\langle X_{\max} \rangle$ (left panel, thick lines), its variance $\sigma(X_{\max})$ (right panel, thick lines) for the model "light" and the corresponding curves for pure proton and Iron composition (thin lines). The hadronic interaction models used are EPOS-LHC (solid lines), QGSJetII-04 (dashed lines), and SIBYLL2.3d (dotted lines). The measurements of Tunka-133, TAIGA-HiSCORE array ([45] open circles), and PAO (energy shift +10% [47], black circles) are also shown.

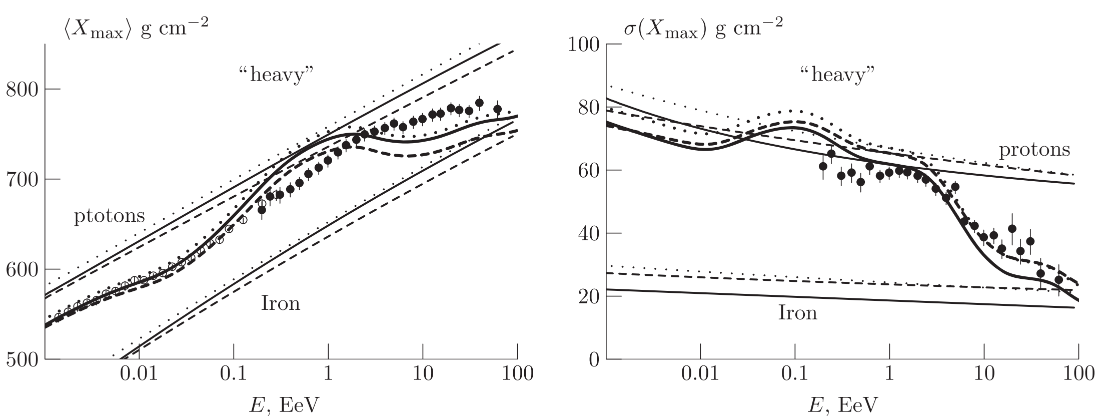

FIG. 6. Similar to Fig. 5, but for model "heavy."

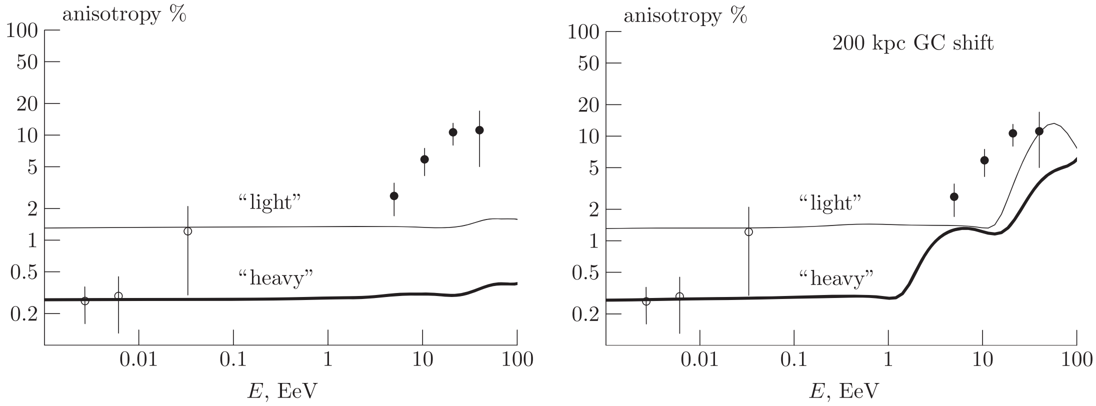

FIG. 7. Calculated cosmic ray anisotropy (solid lines) for the Milky Way situated in the center of the extended halo (left panel) and shifted on 200 kpc in the Andromeda direction (right panel). The results of PAO (energy shift +10%, [48] black circles) and the KASCADE-Grande experiment ([49] open circles) are also shown.

The spectra observed at the Solar System location at the Galactocentric distance $r = R_{\odot} = 8.5$ kpc are shown in Fig. 3. Both models reproduce the observed all-particle spectrum. The "light" model is in better agreement with the observed chemical composition if the interaction model QGSJetII-04 is used (see Figs. 4 and 5). The *unusual* bump at the variance $\sigma(X_{\max})$ curves at the energy 10^{17} eV appears because protons of the intermediary component and Iron nuclei of the bow shock component give the main input in all-particle spectrum at these energies. The Iron nuclei and protons have large difference of the mean depth $\langle X_{\max}\rangle$ and this results in the large variance $\sigma(X_{\max})$. The model "heavy" is preferable for the explanation of the observed anisotropy (see Fig. 7). Relatively high anisotropy at PeV energies in the model "light" is not a serious problem because the anisotropy at these energies is strongly influenced by the local Galactic magnetic fields. This effect is not taken into account in the present study. The numerical value of the calculated anisotropy δ is close to $\delta = 1.5R_{\odot}/cT$ which is the anisotropy of the instantaneous point source in the infinite space. Its value can be higher if the Galaxy is shifted from the halo center (see the right panel of Fig. 7 and the discussion below).

V. DISCUSSION

The maximum energy of particles accelerated at the nonrelativistic bow shock is determined by the nonresonant cosmic ray streaming instability [50] (see Paper I for details),

$$\epsilon^b_{\max} = \frac{\eta_{\rm esc}}{2\ln(B/B_b)} e\sqrt{\beta_{\rm head} L_{\rm j} c^{-1}}$$
$$= 1.73\times 10^{19}\ \mathrm{eV}\frac{\eta_{\rm esc}}{2\ln(B/B_b)}\beta^{1/2}_{\rm head}\left(\frac{L_{\rm j}}{10^{44}\ \mathrm{erg\ s^{-1}}}\right)^{1/2}. \tag{3}$$

Here, $\beta_{\rm head}$ is the ratio of the speed of bow shock "head" to the speed of light c, $L_{\rm j}$ is the total power of two opposite directed jets, and $\eta_{\rm esc}$ is the ratio of the energy flux of runaway accelerated particles to the kinetic flux of the shock. The logarithmic factor in the denominator corresponds to the situation when the seed magnetic field B_b is amplified in the upstream region of the shock up to values of B via cosmic ray streaming instability.

The parameter $\eta_{\rm esc}$ is close to 0.01 for shocks where the pressure of accelerated particles is of the order of 0.1 of the shock ram pressure and can be higher at cosmic-ray-modified shocks. The protons can be accelerated up to multi-PeV energies at the jet bow shocks at $\eta_{\rm esc} = 0.01$, $\beta_{\rm head} = 0.1$ and $\ln(B/B_b) = 5$.

Our modeling shows that particles with energies above 10^{15} eV can be produced in the Galactic Center and observed at the Earth.

Below PeV energies, the particles have no time to reach the Earth and we expect a smooth low energy cutoff of the spectrum. Lower energy particles are probably produced in Galactic supernova remnants. In this regard, our scenario is similar to the model with a nearby source [51]. This model was suggested for the explanation of the "knee" in the observed cosmic ray spectrum. The similar in spirit origin of UHECRs diffusing from the point source in the Galactic Center was also considered in the past [9].

It is known that the electric potential difference is a reasonable estimate for the maximum energy of particles accelerated at quasiperpendicular shocks [52]. For example, single-charged anomalous cosmic rays are accelerated up to hundreds MeV at the solar wind termination shock with the electric potential 200 MV [53]. The jet electric potential is also a good estimate for the maximum energy as seen in trajectory calculations [33,54].

The corresponding value is

$$\epsilon^{j}_{\max} = e\sqrt{\beta_{\mathrm{j}} L_{\mathrm{mag}} c^{-1}} = 1.73 \times 10^{19}\ \mathrm{eV}\beta_{\mathrm{j}}^{1/2} \times \left(\frac{L_{\mathrm{mag}}}{10^{44}\ \mathrm{erg\,s^{-1}}}\right)^{1/2}, \quad (4)$$

where L_{mag} is the magnetic luminosity of two opposite jets; see Paper I for details.

So the jet power $\sim 10^{45}\ \mathrm{erg\,s^{-1}}$ is needed to achieve the maximum energy of 4×10^{19} eV in the "light" model. It means that the Galactic Center SMBH with Eddington luminosity $L_{\mathrm{Edd}} = 5 \times 10^{44}\ \mathrm{erg\,s^{-1}}$ was an Eddington or super-Eddington source during the past active phase. The duration of this phase was only 30 kyrs to supply 10^{57} erg of energy in *eROSITA* bubbles.

A similar jet power is needed in the model of *eROSITA* and *Fermi* bubble formation [55]. In this model, a short energetic event in the Galactic Center 2.6 million years ago produced jets moving in the Galactic halo. After the jet's disappearance, the bow shock of the jet propagated to larger heights and is observed now as the *eROSITA* bubbles. The *Fermi* bubble is a heated jet material inside the eROSITA bubbles. The main difficulty of the model is a high shock speed of 1–2 thousand $\mathrm{km\,s^{-1}}$. The lower shock speed $\sim 350\ \mathrm{km\,s^{-1}}$ was inferred from the gas temperature in *eROSITA* bubbles [5]. However, recent x-ray observations show the presence of more hot gas [56] and the shock speed can be higher.

It was also found that the properties of young stars in the vicinity of Sagittarius A can be explained if they were formed from the massive gas shell ejected by a central energetic super-Eddington outflow 6 million years ago [57]. A similar high ionization energetic event 3.5 million years ago is needed for the explanation of the ionization cones in the Galactic halo [58]. Ionization cones of this kind produced by AGN outburst 65 kyrs ago also exist in the vicinity of Seyfert galaxy NGC 5252 [59].

The last Galactic Center activity was probably distributed in time. For example, it began 15 million years ago with a moderate power and produced the shock with the present speed of $350\ \mathrm{km\,s^{-1}}$. There was an additional powerful energy release at the end of activity 3 million years ago that produced the *Fermi* bubbles. This age of the *Fermi* bubbles is also in agreement with the x-ray absorption study [60].

In this regard the past activity in the Galactic Center is similar to the activity of Narrow Line Seyfert 1 (NLSy 1) galaxies. This Seyfert-like activity with the Eddington luminosity is observed in spiral galaxies with small or moderate SMBHs. About 7 percent of these galaxies have jets. The jets directed to us are similar to blazars and are observed as powerful gamma ray sources [61]. The number of all jetted NLSy 1 galaxies corresponds to the fraction 10^{-4}–10^{-3} of the bright galaxies. This gives an estimate for the duration of an active phase 10^4–10^5 years similar to the parameters of the model "light."

On the other hand, the lower maximum energy in the model "heavy" can be achieved with the jet power of the order of several percent of the Eddington luminosity. The duration of the active phase is close to one million years in this case.

The third intermediate pure proton component produced near the SMBH is closely related to the production of astrophysical neutrinos. This is because it comes from the neutrons generated in $p\gamma$ interactions. The ratio of the total neutron and neutrino energies is close to 5 in this process while the energy of individual neutrinos is 25 times smaller than the neutron energy [62]. This means that the expected metagalactic energy flux of neutrinos is 5 times lower than the one of the corresponding protons. So we can compare the energy flux of metagalactic component at 25 PeV shown in Fig. 3 with the energy flux $\sim 5 \times 10^{-11}\ \mathrm{erg\,cm^{-2}\,s^{-1}\,sr^{-1}}$ of astrophysical neutrinos at PeV energies [31]. We found that for the model "heavy" the expected flux of the astrophysical neutrinos is two times lower than the measured flux.

As for the chemical composition of observed UHECRs the "light" model without a strong enrichment by heavy nuclei looks more attractive. The enrichment is expected in the models with a reacceleration of preexisting low energy cosmic rays in the jet [63,64]. However, it is not easy for background cosmic rays to reach the jet itself because the jet flow is surrounded by an extended region of the heated jet gas (cocoon) and heated at the bow shock interstellar gas (see Fig. 1). In such a situation the reacceleration of particles accelerated at the bow shock might be more probable [16].

Future advances in the investigation of the chemical composition of the highest energy cosmic rays will help to choose the best model. This first concerns the contradictions between the hadronic interaction models (see Figs. 4–6). The dominance of Helium nuclei at the end of the spectrum will be in favor of the Galactic origin of UHECRs (model "light") because Helium nuclei with such energies cannot come from the extragalactic sources. The heavier composition will be in favor of the Galactic model "heavy." An extragalactic origin of UHECRs is also possible in this case.

Further development of more realistic and less phenomenological models for particle acceleration in jets is also needed since there are deviations of experimental and simulated $\langle X_{\max}\rangle$, $\sigma(X_{\max})$ (see Figs. 5 and 6). We leave this problem for future investigations.

A crucial assumption of our model is the strong magnetic field of microgauss strength in the extended halo. For lower values of the field it is impossible to explain the end of the observable spectrum at energies above 10^{18} eV. In this case, a contribution at the highest energies from more distant nearby sources like Cen A radio galaxy [65] or Andromeda galaxy [16] can play a role.

On the other hand if the extended halo with microgauss magnetic fields indeed exists, then the cosmic ray spectrum and chemical composition at energies above 10^{15} eV can be explained by the recent Eddington-like accretion event in the Galactic Center. The assumed jet power 10^{44}–10^{45} erg s^{-1} is 10^3 times higher than the one in our Paper I where the Andromeda galaxy makes the main contribution to the spectrum of UHECRs. Such a high power is possible if the recent accretion event was similar to the activity of NLSy 1 galaxies (see the discussion above). This scenario suggested in the present paper seems to be more probable because it is clear that some strong energy release in the Galactic Center occurred 3–20 million years ago, while the time of the ancient SMBH activity in the Andromeda galaxy is unknown.

The simulated anisotropy is low in the models under consideration. However, this is because we use the spherical simulation domain and observe cosmic rays close to the center. Deviations from the spherical symmetry can result in higher anisotropy, especially at the highest energies.

For example, one can expect such a deviation because of the interaction with the Andromeda galaxy and because our Galaxy is moving in the direction of Andromeda. SMBH in the Andromeda galaxy is 50 times more massive than SMBH in the Galactic Center. So it is expected that outflows driven by AGN activity during the growth of Andromeda's SMBH produced a huge extended halo of the hot gas with a size of several Mpc. The Milky Way's gaseous halo is smaller in size and located inside Andromeda's more extended halo (see Fig. 1). In this situation, we expect that the Galaxy is shifted from its gaseous halo center in the direction of Andromeda. This is because the galactic wind of Andromeda pushed the Galactic halo during its formation. The motion of the Galaxy in the direction of Andromeda produced a similar effect [66]. If the magnetic field is lower in Andromeda's halo, then the highest energy particles produced in the Galactic Center escape easier in the Andromeda direction. The diffusive flux is directed to Andromeda in this case and we expect to see anisotropy from the opposite direction which is approximately the direction of the radio galaxy Cen A. The results for this case are illustrated in the right panel of Fig. 7. The direction of the anisotropy is from the Galactic Center at low energies. It changes to the direction opposite to Andromeda at high energies. Observations of the Auger Collaboration seems to confirm this pattern [48,67].

VI. CONCLUSION

Our conclusions are the following:

(1) We model the propagation of ultrahigh energy particles from the Galactic central source that was active several million years ago and compare the all-particle spectra, anisotropy, and chemical composition obtained with observations. If the active source is less than 3 million years old, the Helium nuclei do not have time for photodisintegration, and a model using the light source composition ("light" model) is possible. For older sources, severe enrichment by heavy nuclei is required to explain the observed spectrum of UHECR ("heavy" model).

(2) The necessary condition for both models is the effective confinement of particles in the extended (several hundred kpc in size) Galactic halo with microgauss magnetic fields. It is expected that this halo was produced by powerful Galactic wind driven by the star formation and SMBH activity of the young Galaxy. The Galactic magnetic fields were transported to the halo and amplified by the Cranfill effect (see the Appendix).

(3) The jet power must be close to the Eddington luminosity in the model "light" to provide a high enough maximum energy of accelerated particles. Such a luminosity is observed at the active phase of jetted NLSy 1 galaxies [61].

(4) We expect that the cosmic ray anisotropy at the highest energies depends on the deviation from spherical symmetry. If this deviation is caused by the interaction with the Andromeda galaxy, the anisotropy can be expected from opposite the Andromeda direction. This is close to the anisotropy pattern observed by the Pierre Auger Observatory.

ACKNOWLEDGMENTS

We thank an anonymous referee for valuable comments and suggestions. The work was partly performed at the Unique scientific installation "Astrophysical Complex of MSU-ISU" (agreement 13.UNU.21.0007).

APPENDIX: MHD MODELING OF THE HOT MAGNETIZED HALO

We performed simplified one-dimensional magnetohydrodynamic (MHD) calculations of the Milky Way halo formation. The effects of rotation and radiative losses are neglected. MHD equations for the gas density $\rho(r,t)$, gas velocity $u(r,t)$, gas pressure $P_g(r,t)$, and magnetic field $B(r,t)$ in the spherically symmetrical case are given by

$$\frac{\partial\rho}{\partial t}+\frac{1}{r^2}\frac{\partial}{\partial r}r^2u\rho=0, \tag{A1}$$

$$\frac{\partial\rho u}{\partial t}+\frac{1}{r^2}\frac{\partial}{\partial r}r^2\left(\rho u^2+P_g+\frac{B^2}{8\pi}\right)=\frac{2P_g}{r}-g(r)\rho, \tag{A2}$$

$$\frac{\partial\varepsilon}{\partial t}+\frac{1}{r^2}\frac{\partial}{\partial r}r^2u\left(\varepsilon+P_g+\frac{B^2}{8\pi}\right)=-g(r)\rho u, \tag{A3}$$

$$\frac{\partial B}{\partial t}+\frac{1}{r}\frac{\partial Bur}{\partial r}=0, \tag{A4}$$

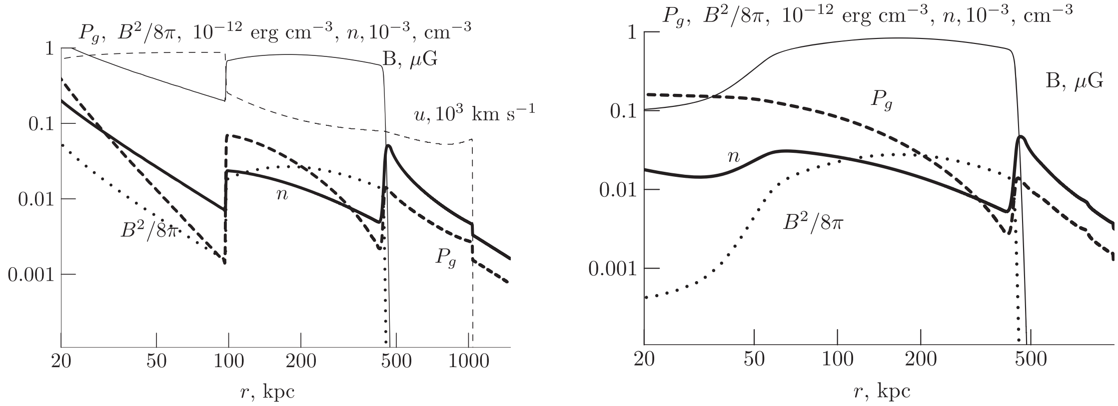

FIG. 8. The radial dependence of the gas density (thick solid line), the gas velocity (thin dashed line), the magnetic energy density $B^2/8\pi$ (dotted line), the magnetic field strength B (thin solid line), and the gas pressure P_g (thick dashed line) at $t = 5$ Gyr (left panel) and at the current epoch $t = 13.7$ Gyr (right panel).

where $\varepsilon = \frac{1}{2}\rho u^2 + \frac{P_g}{\gamma_g - 1} + \frac{B^2}{8\pi}$ is the total energy density and $\gamma_g = 5/3$ is the adiabatic index of the gas. Equations (A1)–(A3) are the continuity equation, the momentum equation, and the energy equation, respectively, while Eq. (A4) describes the evolution of the nonradial components of the magnetic field.

The gravitational acceleration $g(r) = V_c^2/r$ is dominated by the dark matter of the virialized isothermal halo with parameter $V_c \approx 200$ km s^{-1}. At the initial instant of time $t_0 = 1$ Gyr after the Big Bang the density and gas pressure are given by the expressions

$$\rho = \frac{\eta_b V_c^2}{4\pi G R_h^2} \begin{cases} 1, r < R_h \\ R_h^2/r^2, r > R_h, \end{cases} \tag{A5}$$

$$P_g = \frac{\eta_b V_c^4}{8\pi G R_h^2} \begin{cases} (1 + 2\ln(R_h/r)), r < R_h \\ R_h^2/r^2, r > R_h. \end{cases} \tag{A6}$$

Here, G is the gravitational constant and $\eta_b \approx \frac{1}{6}$ is the baryon fraction. This initial matter distribution corresponds to the situation when the gas in the central part of the virialized halo at $r < R_h \approx 150$ kpc was cooled radiatively and formed the Galaxy in the center. Half of this mass $\sim 10^{11} M_\odot$ will be ejected later, leaving the Galaxy with a baryon deficit ("missing" baryons [68]).

The Eqs. (A1)–(A4) are solved numerically at $r > R_0 = 15$ kpc. We use the Total Variation Diminishing hydrodynamic scheme [69] with "minmod" flux limiter. The mass loss rate $25 M_\odot$ yr^{-1} and energy power 8×10^{42} erg s^{-1} are fixed during 4 Gyr at the inner boundary at $r = R_0$. This release of 10^{60} erg of energy and $10^{11} M_\odot$ of matter results in a powerful outflow (Galactic wind) with the speed of about 900 km s^{-1}. Its magnetization is provided by the magnetic source at the inner boundary. Its strength is adjusted to obtain the Mach number $M_a = u/V_a = 4$ of the wind. The sources are switched off after $t = 5$ Gyr.

Figure 8 illustrates the results. The hydrodynamical profiles at the end of the energy release at $t = 5$ Gyr are shown in the left panel. The magnetic field is compressed at the termination shock at $r = 100$ kpc and is further amplified by the Cranfill effect. As a result, the magnetic pressure is higher than the gas pressure at the edge of the cavity at $r \sim 500$ kpc. The expansion of the cavity drives an outer shock at $r \sim 1$ Mpc. At later times the termination shock goes back to the Galaxy, the reflected shock makes several oscillations and the system goes to the quasisteady state at the current epoch—see the right panel. Probably a weak additional release of energy and matter at $t > 5$ Gyr could result in higher values of the density and magnetic field at distances $r < 100$ kpc but can not change the magnetic field and density distribution at larger distances. We conclude that the microgauss magnetic fields in the huge Galactic halo are indeed possible.

The final value of the halo magnetic field can be lower for higher values of the Mach number M_a that is for the lower Galactic wind magnetization. Probably this explains lower values of the magnetic field strength $B \sim 0.1$ μG found in 3D MHD cosmological simulations of Milky Way-like galaxies [70]. The corresponding simulated rotation measure is lower than the recently measured Faraday rotation for different samples of galaxies [39,40]. In addition, in a real three-dimensional geometry the shell of the cavity is unstable relative to the Rayleigh-Taylor instability, and "fingers" and clouds of the denser outer gas penetrate the cavity.

[1] A. Bykov, N. Gehrels, H. Krawczynski, M. Lemoine, G. Pelletier, and M. Pohl, Particle acceleration in relativistic outflows, Space Sci. Rev. **173**, 309 (2012).
[2] F. M. Rieger, Active Galactic nuclei as potential sources of ultra-high energy cosmic rays, Universe **8**, 607 (2022).
[3] N. Globus and R. Blandford, Ultra high energy cosmic ray source models: Successes, challenges and general predictions, EPJ Web Conf. **283**, 04001 (2023).
[4] M. Su, T. R. Slatyer, and D. P. Finkbeiner, Giant gamma-ray bubbles from Fermi-LAT: Active Galactic nucleus activity or bipolar Galactic wind?, Astrophys. J. **724**, 1044 (2010).
[5] P. Predehl, R. A. Sunyaev, W. Becker, H. Brunner, R. Burenin, A. Bykov *et al.*, Detection of large-scale X-ray bubbles in the Milky Way halo, Nature (London) **588**, 227 (2020).
[6] A. Pillepich, D. Nelson, N. Truong, R. Weinberger, I. Martin-Navarro, V. Springel *et al.*, X-ray bubbles in the circumgalactic medium of TNG50 Milky Way- and M31-like galaxies: Signposts of supermassive black hole activity, Mon. Not. R. Astron. Soc. **508**, 4667 (2021).
[7] C.-Y. Fan, On Fermi's theory of the origin of cosmic radiation, Phys. Rev. **82**, 211 (1951).
[8] G. R. Burbidge and F. Hoyle, The Galactic halo-A transient phenomenon, Astrophys. J. **138**, 57 (1963).
[9] G. V. Kulikov, Y. A. Fomin, and G. B. Khristiansen, New possibility of explaining the complex form of the energy spectrum of ultrahigh energy primary cosmic rays, JETP Lett. **10**, 222 (1969).
[10] J. R. Wayland, Pulsed Galactic nuclei and the origin of cosmic rays, Astrophys. Space Sci. **18**, 89 (1972).
[11] V. S. Ptuskin and Y. M. Khazan, The Galactic center and the origin of cosmic rays, Sov. Astron. **25**, 547 (1981).
[12] M. Giler, Cosmic rays from the Galactic centre, J. Phys. G **9**, 1139 (1983).
[13] Y. Istomin, On the origin of Galactic cosmic rays, New Astron. **27**, 13 (2014).
[14] Y. Fujita, K. Murase, and S. S. Kimura, Sagittarius A* as an origin of the Galactic PeV cosmic rays?, J. Cosmol. Astropart. Phys. 04 (2017) 037.
[15] Á. Bogdán and M. Vogelsberger, X-ray halos around massive galaxies: Data and theory, in *Handbook of X-ray and Gamma-ray Astrophysics*, edited by C. Bambi and A. Santangelo (Springer Nature, Singapore, 2022), pp. 1–30.
[16] V. N. Zirakashvili, V. S. Ptuskin, and S. I. Rogovaya, Ultra high energy cosmic rays from past activity of Andromeda galaxy, Mon. Not. R. Astron. Soc. **519**, L5 (2023).
[17] G. F. Krymskii, A regular mechanism for the acceleration of charged particles on the front of a shock wave, Sov. Phys. Dokl. **22**, 327 (1977).
[18] A. R. Bell, The acceleration of cosmic rays in shock fronts —I, Mon. Not. R. Astron. Soc. **182**, 147 (1978).
[19] W. I. Axford, E. Leer, and G. Skadron, The acceleration of cosmic rays by shock waves, in *International Cosmic Ray Conference* (Central Research Institute for Physics of the Hungarian Academy of Sciences, 1977), Vol. 11, p. 132.
[20] R. D. Blandford and J. P. Ostriker, Particle acceleration by astrophysical shocks, Astrophys. J. Lett. **221**, L29 (1978).
[21] E. G. Berezhko, Acceleration of charged particles in a cosmic-phase shear flow, Sov. Phys. JETP **33**, 416 (1981).
[22] J. A. Earl, J. R. Jokipii, and G. Morfill, Cosmic-ray viscosity, Astrophys. J. Lett. **331**, L91 (1988).
[23] Y. N. Istomin and H. Sol, Acceleration of particles in the vicinity of a massive black hole, Astrophys. Space Sci. **321**, 57 (2009).
[24] M. Bañados, J. Silk, and S. M. West, Kerr black holes as particle accelerators to arbitrarily high energy, Phys. Rev. Lett. **103**, 111102 (2009).
[25] T. Jacobson and T. P. Sotiriou, Spinning black holes as particle accelerators, Phys. Rev. Lett. **104**, 021101 (2010).
[26] S.-W. Wei, Y.-X. Liu, H. Guo, and C.-E. Fu, Charged spinning black holes as particle accelerators, Phys. Rev. D **82**, 103005 (2010).
[27] D. Caprioli, D. T. Yi, and A. Spitkovsky, Chemical enhancements in shock-accelerated particles: *Ab initio* simulations, Phys. Rev. Lett. **119**, 171101 (2017).
[28] M. G. Revnivtsev, E. M. Churazov, S. Yu. Sazonov, R. A. Sunyaev, A. A. Lutovinov, M. R. Gilfanov, A. A. Vikhlinin, P. E. Shtykovsky, and M. N. Pavlinsky, Hard X-ray view of the past activity of Sgr A* in a natural Compton mirror, Astron. Astrophys. **425**, L49 (2004).
[29] J. Seo, H. Kang, and D. Ryu, A simulation study of ultra-relativistic jets. II. structures and dynamics of FR-II jets, Astrophys. J. **920**, 144 (2021).
[30] R. Blandford, D. Meier, and A. Readhead, Relativistic jets from active Galactic nuclei, Annu. Rev. Astron. Astrophys. **57**, 467 (2019).
[31] S. V. Troitsky, Constraints on models of the origin of high-energy astrophysical neutrinos, Phys. Usp. **64**, 1261 (2021).
[32] V. S. Berezinsky, Extraterrestial neutrino sources and high energy neutrino astrophysics, in *Neutrino '77: Proceedings of the International Conference on Neutrino Physics and Neutrino Astrophysics* (Nauka, 1978), p. 177.
[33] E. P. Alves, J. Zrake, and F. Fiuza, Efficient nonthermal particle acceleration by the kink instability in relativistic jets, Phys. Rev. Lett. **121**, 245101 (2018).
[34] D. Harari, S. Mollerach, and E. Roulet, Anisotropies of ultrahigh energy cosmic rays diffusing from extragalactic sources, Phys. Rev. D **89**, 123001 (2014).
[35] A. Arámburo-García, K. Bondarenko, A. Boyarsky, D. Nelson, A. Pillepich, and A. Sokolenko, Magnetization of the intergalactic medium in the IllustrisTNG simulations: The importance of extended, outflow-driven bubbles, Mon. Not. R. Astron. Soc. **505**, 5038 (2021).
[36] H. J. Völk and A. M. Atoyan, Early starbursts and magnetic field generation in galaxy clusters, Astrophys. J. **541**, 88 (2000).
[37] W. I. Axford, *The Interaction of the Solar Wind with the Interstellar Medium*, edited by C. P. Sonett, P. J. Coleman, and J. M. Wilcox (NASA Special Publication, 1972), Vol. 308, p. 609.
[38] C. W. Cranfill, Flow problems in astrophysical systems, Ph.D. thesis, University of California, San Diego, 1974.
[39] V. Heesen, S. P. O'Sullivan, M. Brüggen, A. Basu, R. Beck, A. Seta *et al.*, Detection of magnetic fields in the circumgalactic medium of nearby galaxies using Faraday rotation, Astron. Astrophys. **670**, L23 (2023).
[40] K. Böckmann, M. Brüggen, V. Heesen, A. Basu, S. P. O'Sullivan, I. Heywood *et al.*, Probing magnetic fields in

the circumgalactic medium using polarization data from MIGHTEE, Astron. Astrophys. **678**, A56 (2023).

[41] M. De Domenico, M. Settimo, S. Riggi, and E. Bertin, Reinterpreting the development of extensive air showers initiated by nuclei and photons, J. Cosmol. Astropart. Phys. 07 (2013) 050.

[42] A. Abdul Halim, P. Abreu, M. Aglietta, I. Allekotte, K. Almeida Cheminant, A. Almela *et al.*, Constraining the sources of ultra-high-energy cosmic rays across and above the ankle with the spectrum and composition data measured at the Pierre Auger Observatory, J. Cosmol. Astropart. Phys. 05 (2023) 024.

[43] N. M. Budnev, A. Chiavassa, O. A. Gress, T. I. Gress, A. N. Dyachok, N. I. Karpov *et al.*, The primary cosmic-ray energy spectrum measured with the Tunka-133 array, Astropart. Phys. **117**, 102406 (2020).

[44] Pierre Auger Collaboration, The energy spectrum of cosmic rays beyond the turn-down around 10^{17} eV as measured with the surface detector of the Pierre Auger Observatory, Eur. Phys. J. C **81**, 966 (2021).

[45] V. Prosin, I. Astapov, P. Bezyazeekov, E. Bonvech, A. Borodin, A. Bulan *et al.*, Primary cosmic rays energy spectrum and mean mass composition by the data of the TAIGA astrophysical complex, SciPost Phys. Proc. **13**, 037 (2023).

[46] J. Bellido, A. Aab, P. Abreu, M. Aglietta, I. F. M. Albuquerque *et al.* (The Pierre Auger Collaboration), Depth of maximum of air-shower profiles at the Pierre Auger Observatory: Measurements above $10^{17.2}$ eV and Composition Implications, in The Pierre Auger Observatory: Contributions to the 35th International Cosmic Ray Conference (ICRC 2017) (2017), arXiv:1708.06592.

[47] A. Yushkov, Mass composition of cosmic rays with energies above 10(17.2) eV from the hybrid data of the Pierre Auger Observatory, in *36th International Cosmic Ray Conference (ICRC2019)* (2019), Vol. 36, p. 482.

[48] A. Aab, P. Abreu, M. Aglietta, I. F. M. Albuquerque, J. M. Albury, I. Allekotte *et al.*, Large-scale cosmic-ray anisotropies above 4 EeV measured by the Pierre Auger Observatory, Astrophys. J. **868**, 4 (2018).

[49] A. Chiavassa, W. D. Apel, J. C. Arteaga-Velázquez, K. Bekk, M. Bertaina, J. Blümer *et al.*, A study of the first harmonic of the large scale anisotropies with the KASCADE-Grande experiment, in *34th International Cosmic Ray Conference (ICRC2015)* (2015), Vol. 34, p. 281.

[50] A. R. Bell, Turbulent amplification of magnetic field and diffusive shock acceleration of cosmic rays, Mon. Not. R. Astron. Soc. **353**, 550 (2004).

[51] A. D. Erlykin and A. W. Wolfendale, A single source of cosmic rays in the range 10^{15}–10^{16} ev, J. Phys. G **23**, 979 (1997).

[52] V. Zirakashvili and V. Ptuskin, Cosmic ray acceleration in magnetic circumstellar bubbles, Astropart. Phys. **98**, 21 (2018).

[53] A. C. Cummings and E. C. Stone, Energy spectra of anomalous cosmic-ray oxygen during 1977-1987, in International Cosmic Ray Conference (1987), Vol. **3**, p. 421.

[54] R. Mbarek and D. Caprioli, Bottom-up acceleration of ultra-high-energy cosmic rays in the jets of active Galactic nuclei, Astrophys. J. **886**, 8 (2019).

[55] H. Y. K. Yang, M. Ruszkowski, and E. G. Zweibel, Fermi and eROSITA bubbles as relics of the past activity of the Galaxy's central black hole, Nat. Astron. **6**, 584 (2022).

[56] A. Gupta, S. Mathur, J. Kingsbury, S. Das, and Y. Krongold, Thermal and chemical properties of the eROSITA bubbles from Suzaku observations, Nat. Astron. **7**, 799 (2023).

[57] S. Nayakshin and K. Zubovas, Sgr A* envelope explosion and the young stars in the centre of the Milky Way, Mon. Not. R. Astron. Soc. **478**, L127 (2018).

[58] J. Bland-Hawthorn, P. R. Maloney, R. Sutherland, B. Groves, M. Guglielmo, W. Li, A. Curzons, G. Cecil, and A. J. Fox, The large-scale ionization cones in the galaxy, Astrophys. J. **886**, 45 (2019).

[59] C. Wang, J. Wang, M. Dadina, G. Fabbiano, M. Elvis, S. Bianchi, and M. Guainazzi, Deep Chandra observation of the remarkable ionization cones of NGC 5252, Astrophys. J. **962**, 188 (2024).

[60] M. J. Miller and J. N. Bregman, The interaction of the Fermi bubbles with the Milky Way's hot gas halo, Astrophys. J. **829**, 9 (2016).

[61] F. D'Ammando, Relativistic jets in gamma-ray-emitting narrow-line Seyfert 1 galaxies, Galaxies **7**, 87 (2019).

[62] A. Mücke, J. P. Rachen, R. Engel, R. J. Protheroe, and T. Stanev, Photomeson production in astrophysical sources, Nucl. Phys. B, Proc. Suppl. **80**, 0810 (2000).

[63] D. Caprioli, "Espresso" acceleration of ultra-high-energy cosmic rays, Astrophys. J. Lett. **811**, L38 (2015).

[64] S. S. Kimura, K. Murase, and B. T. Zhang, Ultrahigh-energy cosmic-ray nuclei from black hole jets: Recycling Galactic cosmic rays through shear acceleration, Phys. Rev. D **97**, 023026 (2018).

[65] S. Mollerach and E. Roulet, Ultrahigh energy cosmic rays from a nearby extragalactic source in the diffusive regime, Phys. Rev. D **99**, 103010 (2019).

[66] R. Weaver, R. McCray, J. Castor, P. Shapiro, and R. Moore, Interstellar bubbles. II. Structure and evolution, Astrophys. J. **218**, 377 (1977).

[67] J. Biteau, P. Abreu, M. Aglietta, J. M. Albury, I. Allekotte *et al.* (The Pierre Auger Collaboration), The ultra-high-energy cosmic-ray sky above 32 EeV viewed from the Pierre Auger Observatory, in *37th International Cosmic Ray Conference* (2022), p. 307.

[68] S. S. McGaugh, J. M. Schombert, W. J. G. de Blok, and M. J. Zagursky, The baryon content of cosmic structures, Astrophys. J. Lett. **708**, L14 (2010).

[69] H. Trac and U.-L. Pen, A primer on Eulerian computational fluid dynamics for astrophysics, Publ. Astron. Soc. Pac. **115**, 303 (2003).

[70] R. Pakmor, F. van de Voort, R. Bieri, F. A. Gómez, R. J. J. Grand, T. Guillet, F. Marinacci, C. Pfrommer, C. M. Simpson, and V. Springel, Magnetizing the circumgalactic medium of disc galaxies, Mon. Not. R. Astron. Soc. **498**, 3125 (2020).